Silicon-Germanium multi-quantum well photodetectors in the near infrared

Efe Onaran,[1,*] M. Cengiz Onbasli,[2] Alper Yesilyurt,[1] Hyun Yong Yu,[3] Ammar M. Nayfeh,[4] and Ali K. Okyay[1,5,6]

[1]Department of Electrical and Electronics Engineering, Bilkent University, Ankara 06800, Turkey
[2]Department of Materials Science and Engineering, Massachusetts Institute of Technology, Cambridge, Massachusetts 02139, USA
[3]The School of Electrical Engineering, Korea University, Seoul, South Korea
[4]Masdar Institute of Science and Technology, Abu Dhabi, UAE
[5]UNAM, Institute of Materials Science and Nanotechnology, Bilkent University, Ankara 06800, Turkey
[6]aokyay@ee.bilkent.edu.tr
[*]e_onaran@ug.bilkent.edu.tr

Abstract: Single crystal Silicon-Germanium multi-quantum well layers were epitaxially grown on silicon substrates. Very high quality films were achieved with high level of control utilizing recently developed MHAH epitaxial technique. MHAH growth technique facilitates the monolithic integration of photonic functionality such as modulators and photodetectors with low-cost silicon VLSI technology. Mesa structured *p-i-n* photodetectors were fabricated with low reverse leakage currents of ~10 mA/cm^2 and responsivity values exceeding 0.1 A/W. Moreover, the spectral responsivity of fabricated detectors can be tuned by applied voltage.

©2012 Optical Society of America

OCIS codes: (230.5160) Photodetectors; (230.5590) Quantum-well, -wire and -dot devices; (230.4205) Multiple quantum well (MQW) modulators; (160.2100) Electro-optical materials.

References and links

1. J. Mathews, R. Roucka, J. Xie, S.-Q. Yu, J. Menéndez, and J. Kouvetakis, "Extended performance GeSn/Si(100) p-i-n photodetectors for full spectral range telecommunication applications," Appl. Phys. Lett. **95**(13), 133506 (2009).
2. A. M. Nayfeh, C. O. Chui, K. C. Saraswat, and T. Yonehara, "Effects of hydrogen annealing on heteroepitaxial-Ge layers on Si: surface roughness and electrical quality," Appl. Phys. Lett. **85**(14), 2815–2817 (2004).
3. A. K. Okyay, A. M. Nayfeh, K. C. Saraswat, T. Yonehara, A. Marshall, and P. C. McIntyre, "High-efficiency metal-semiconductor-metal photodetectors on heteroepitaxially grown Ge on Si," Opt. Lett. **31**(17), 2565–2567 (2006).
4. O. Fidaner, A. K. Okyay, J. E. Roth, R. K. Schaevitz, Y.-H. Kuo, K. C. Saraswat, J. S. Harris, and D. A. B. Miller, "Ge–SiGe quantum-well waveguide photodetectors on silicon for the near-infrared," IEEE Photon. Technol. Lett. **19**(20), 1631–1633 (2007).
5. H.-Y. Yu, S. Ren, W. S. Jung, A. K. Okyay, D. A. B. Miller, and K. C. Saraswat, "High-efficiency p-i-n photodetectors on selective-area-grown Ge for monolithic integration," IEEE Electron Device Lett. **30**(11), 1161–1163 (2009).
6. S. B. Samavedam, M. T. Currie, T. A. Langdo, and E. A. Fitzgerald, "High-quality germanium photodiodes integrated on silicon substrates using optimized relaxed graded buffers," Appl. Phys. Lett. **73**(15), 2125–2127 (1998).
7. J. L. Liu, Z. Yang, and K. L. Wang, "Sb surfactant-mediated SiGe graded layers for Ge photodiodes integrated on Si," J. Appl. Phys. **99**(2), 024504 (2006).
8. M. Oehme, J. Werner, E. Kasper, M. Jutzi, and M. Berroth, "High bandwidth Ge p-i-n photodetector integrated on Si," Appl. Phys. Lett. **89**(7), 071117 (2006).
9. J. Liu, J. Michel, W. Giziewicz, D. Pan, K. Wada, D. D. Cannon, S. Jongthammanurak, D. T. Danielson, L. C. Kimerling, J. Chen, F. Ö. Ilday, F. X. Kärtner, and J. Yasaitis, "High-performance, tensile-strained Ge p-i-n photodetectors on a Si platform," Appl. Phys. Lett. **87**(10), 103501 (2005).
10. L. Colace, M. Balbi, G. Masini, G. Assanto, H.-C. Luan, and L. C. Kimerling, "Ge on Si p-i-n photodiodes operating at 10 Gbit/s," Appl. Phys. Lett. **88**(10), 101111 (2006).
11. S. Famà, L. Colace, G. Masini, G. Assanto, and H.-C. Luan, "High performance germanium-on-silicon detectors

for optical communications," Appl. Phys. Lett. **81**(4), 586–588 (2002).

12. D. Ahn, C. Y. Hong, J. Liu, W. Giziewicz, M. Beals, L. C. Kimerling, J. Michel, J. Chen, and F. X. Kärtner, "High performance, waveguide integrated Ge photodetectors," Opt. Express **15**(7), 3916–3921 (2007).
13. L. Vivien, J. Osmond, J.-M. Fédéli, D. Marris-Morini, P. Crozat, J.-F. Damlencourt, E. Cassan, Y. Lecunff, and S. Laval, "42 GHz p.i.n Germanium photodetector integrated in a silicon-on-insulator waveguide," Opt. Express **17**(8), 6252–6257 (2009).
14. B. Li, G. Li, E. Liu, Z. Jiang, J. Qin, and X. Wang, "Monolithic integration of a SiGe/Si modulator and multiple quantum well photodetector for 1.55 μm operation," Appl. Phys. Lett. **73**(24), 3504–3505 (1998).
15. Y.-H. Kuo, Y. K. Lee, Y. Ge, S. Ren, J. E. Roth, T. I. Kamins, D. A. B. Miller, and J. S. Harris, "Strong quantum-confined Stark effect in germanium quantum-well structures on silicon," Nature **437**(7063), 1334–1336 (2005).
16. D. Miller, D. Chemla, T. Damen, A. Gossard, W. Wiegmann, T. Wood, and C. Burrus, "Band-edge electroabsorption in quantum well structures: the quantum-confined Stark effect," Phys. Rev. Lett. **53**(22), 2173–2176 (1984).
17. D. A. B. Miller, D. S. Chemla, T. C. Damen, A. C. Gossard, W. Wiegmann, T. H. Wood, and C. A. Burrus, "Electric field dependence of optical absorption near the band gap of quantum-well structures," Phys. Rev. B Condens. Matter **32**(2), 1043–1060 (1985).
18. C. Chen, B. Yu, J. Liu, and Q. Dai, "Structural characteristics of SiGe/Si materials investigated by Raman spectroscopy," Met. Mater. Int. **11**(4), 279–283 (2005).
19. J. Olivares, P. Martin, A. Rodriguez, J. Sangrador, J. Jimenez, and T. Rodríguez, "Raman spectroscopy study of amorphous SiGe films deposited by low pressure chemical vapor deposition and polycrystalline SiGe films obtained by solid-phase crystallization," Thin Solid Films **358**(1–2), 51–56 (2000).
20. H.-C. Luan, K. Wada, L. C. Kimerling, G. Masini, L. Colace, and G. Assanto, "High efficiency photodetectors based on high quality epitaxial germanium grown on silicon substrates," Opt. Mater. **17**(1-2), 71–73 (2001).
21. P. R. Bandaru, S. Sahni, E. Yablonovitch, J. Liu, H.-J. Kim, and Y.-H. Xie, "Fabrication and characterization of low temperature (<450 °C) grown p-Ge/n-Si photodetectors for silicon based photonics," Mater. Sci. Eng. B **113**(1), 79–84 (2004).
22. L. Colace, P. Ferrara, G. Assanto, D. Fulgoni, and L. Nash, "Low dark-current germanium-on-silicon near-infrared detectors," IEEE Photon. Technol. Lett. **19**(22), 1813–1815 (2007).

1. Introduction

The established silicon (Si) complementary metal-oxide semiconductor (CMOS) technology provides a low-cost platform and reproducible fabrication capabilities for on-chip optical and electronic signal processing. Integrated light detectors and modulators offer added functionality to modern integrated circuits (ICs). Compound semiconductor-based devices (e.g. InGaAs) enjoy high performance. Stringent market requirements drive the development of lower-cost and easier-to-integrate SiGe optoelectronic device technology. While compound semiconductor optoelectronic devices operate with relatively high performance, SiGe-based optoelectronic devices offer ease of processing and integration with electronics, low cost and strain tunability. Germanium is a promising semiconductor compatible with both CMOS and Group III-V technologies and it is sensitive at standard telecommunication bands (C-band, L-band) where Si is transparent [1]. Using Si as a platform, growth of Ge-on-Si enables the low-cost integration of optoelectronics and CMOS technologies. Monolithic integration of optoelectronic devices on-chip with higher density and increased functionality thus becomes possible.

Direct growth of Ge on Si is challenging due to the mismatch of lattice parameters and thermal expansion coefficients of Ge and Si, causing threading dislocations to propagate from the interface and leading to poor device performance or complete device failure. Recently, Nayfeh and associates developed multiple hydrogen annealing heteroepitaxy (MHAH) that enables low dislocation-density Ge growth on Si [2–5].

Epitaxial germanium on silicon for photodetection by graded buffer layers [6, 7], molecular beam epitaxy [8], a two-step growth by ultra-high vacuum chemical vapor deposition (UHVCVD) [9, 10], and cyclic thermal annealing to reduce dislocation density in grown films were reported [11–13]. Metal-semiconductor-metal (MSM) and *p-i-n* type optical detectors were previously fabricated on blanket [3], and selective area grown germanium on silicon by MHAH technique are also reported earlier [5]. Low germanium content SiGe modulator devices were integrated with detectors [14]. Recently, Kuo and

associates demonstrated Ge-rich SiGe electroabsorption modulators based on quantum confined Stark effect (QCSE) [15]. Monolithic integration of modulators and optical detectors with silicon readout integrated circuits (ROIC) paves the way for optical functionality on silicon ICs for near infrared imaging and communications, low cost spectroscopy applications, and hyperspectral imaging applications. For such applications, Si compatible optical detectors with tunable spectral responses could provide significant performance and cost advantage. Pure epitaxial Germanium layers are demonstrated for near-infrared sensitive photodetectors, but their spectral responsivity characteristics cannot be tuned efficiently with external voltage bias. Thin Ge quantum wells obtained on a Ge-on-Si platform (i) increase light absorption owing to strained lattice, (ii) provide tunability of device operation wavelength by changing the bi-layer thickness of each quantum well-and-barrier pair and (iii) increase modulation depth with quantum-confined Stark effect, which is stronger than Franz-Keldysch effect observed in bulk semiconductors [16, 17]. Earlier, we have shown waveguide detectors employing SiGe multi-quantum-wells (MQWs) [4], however, such devices require typically 10V of bias and may suffer from large RC time constants related with the relatively large size of waveguide structures. In this work, we report the growth of very thin Ge-SiGe MQWs as well as fabrication and optoelectronic characterization of high performance *p-i-n* optical detectors on such layers.

2. Device fabrication

P-type (100) silicon wafers were cleaned with standard organic cleaning in 4:1 H_2SO_4:H_2O_2 at 120°C for 20 min followed by removal of chemical oxide in 50:1 H_2O:HF. Trace metals were removed by 5:1:1 H_2O:H_2O_2:HCl mixture at 70°C. A last step of oxide removal was performed in 50:1 H_2O:HF followed by immediately loading into an Applied Materials reduced pressure epitaxial reactor. The wafers were baked in H_2 ambient at 1000°C for 5 minutes followed by the growth of an ultra-thin seed Silicon layer at 700°C. The seed layer provides a very clean surface to start Ge growth. Temperature was lowered to 400°C and a 180-nm-thick p-type Ge buffer layer was grown. Wafer temperature was ramped up to 825°C and baked for 20 min in H_2 ambient. This step allows surface reconstruction before further Ge growth. The presence of H_2 enhances diffusion of species making the surface smoother in addition to dislocation annihilation by gliding during this anneal. The temperature was set to 400°C once again and the previous growth and anneal steps were repeated, resulting in a virtual Ge substrate. Subsequent growth (without intermediate annealing steps) is performed to obtain undoped quantum well and barrier layers. 10 pairs of alternating Ge well regions and Si-Ge barrier regions were grown at 400°C. Intermediate annealing was avoided to prevent any inter-diffusion of (i) Si and Ge and (ii) impurities from underlying highly doped regions. Finally, a 100-nm-thick n-type Ge layer was grown at 400°C as a cap layer and to provide ohmic contact to the Si-Ge *p-i-n* MQW. Figure 1 shows the cross-sectional transmission electron microscope (TEM) image of the MQW layers and Table 1 lists the corresponding layer thicknesses. Compositional depth profiles of the grown layers are obtained by X-ray photoelectron spectroscopy (XPS) study. The samples were etched and in situ measured periodically in time. Photoelectron signal was recorded between every etch cycle using Thermo K-Alpha monochromated XPS Spectrometer. Figure 2 shows the obtained Si and Ge composition vs. etching time profile while carbon and oxygen signals were below measurable limits. XPS study shows that the barrier regions are $Si_{0.08}Ge_{0.92}$ throughout the MQW structure that verifies minimal interdiffusion of Si and Ge.
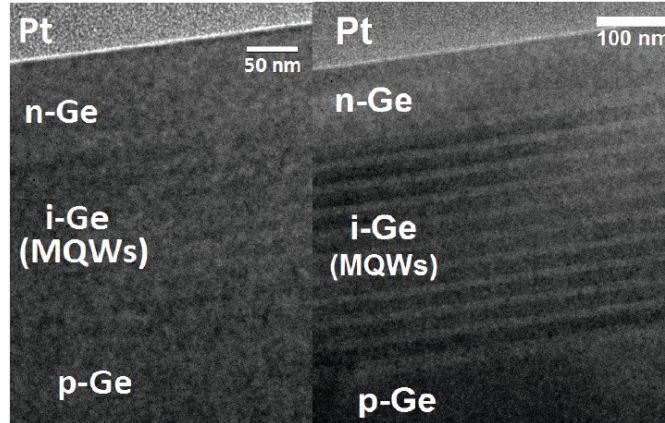
Fig. 1. Cross sectional transmission electron microscope (TEM) image of grown SiGe *p-i-n* MQW structure.
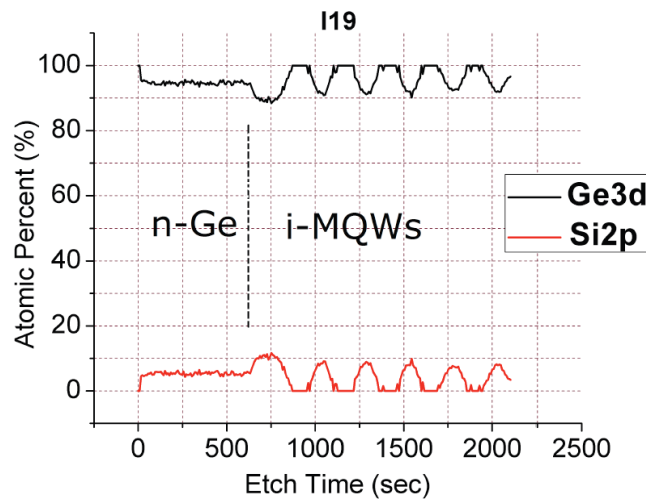

Fig. 2. Compositional depth profile of grown SiGe *p-i-n* MQW structure obtained by X-ray photoelectron spectroscopy (XPS) and in situ etching.

Table 1. *p-i-n* MQW architectures (10 MQW pairs)

Layers	I19 ~layer thickness (nm)		
n-type Ge	100		
Intrinsic (Ge MQWs) (10 pairs)	300	Ge well (each)	10 nm
		$Si_{0.1}Ge_{0.9}$ barrier (each)	20 nm
p-type Ge	370		

Photoluminescence (PL) spectrum is measured to observe the crystalline quality of *p-i-n* MQW structures and probe available energy states and allowed transitions between the states. PL measurements were obtained by light excitation at λ = 225 nm. The layers have sharp luminescence peaks at 425 nm and 500 nm, as shown in Fig. 3. Raman spectroscopy is performed to investigate phonon modes of the system. Typical Raman spectrum of a Ge/Si_xGe_{1-x} system involves Ge-Ge, Ge-Si and Si-Si vibrational modes and depends on the film thickness, stress, material content and quality [18]. The shifted energy of excitation photons of 532 nm gives information about the material composition as shown in Fig. 4. The penetration depth of such excitation enables us to get information about the Ge and Si_xGe_{1-x}

(x = 0.1) layers. Ge-Ge peak (~297 cm^{-1}) corresponds to the Raman shift associated with Ge-rich layers. Furthermore, Si-Ge (~385 cm^{-1}) and Si-Si (~450 cm^{-1}) peaks represent the Si-Ge and Si-Si bonds of Si$_x$Ge$_{1-x}$ layers. Peak positions are highly consistent with the linear fit equations acquired with compositional analysis of Si$_x$Ge$_{1-x}$ layers [19]. Note that, (Si-Si) Raman shift peak of bulk Si is not observed due to poor penetration.
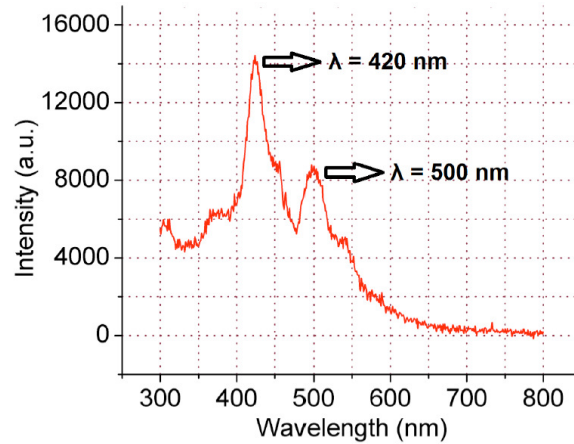
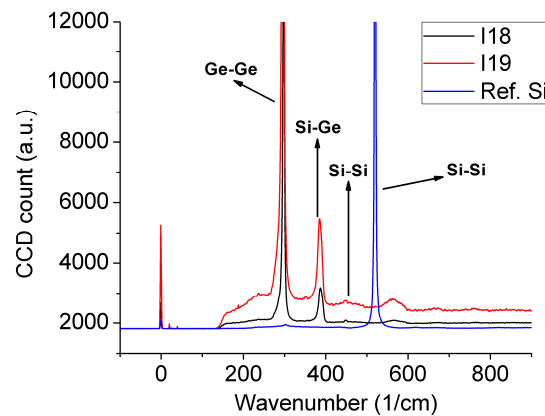Fig. 3. Photoluminescence spectra of SiGe *p-i-n* MQW (excitation wavelength is 225 nm).

Fig. 4. Raman signal obtained for reference Si and SiGe MQW layers.

MQW samples were patterned in disc shaped mesas using standard UV photolithography, etched with SF$_6$ gas at a rate of 175 nm/min down to highly doped Si substrate to become circular mesa structures for detector mode operation. Mesa structures were chosen with respect to other electrode topologies (i.e. planar interdigitated electrodes) since (i) vertical photocurrent collection isolates the photodetector from remaining surface of substrate and thus reduces surface leakage current and (ii) fringing fields are mostly avoided and almost all of the E-field bias participates into charge separation and collection. A 200-nm-thick conformal Si$_3$N$_4$ layer was deposited with plasma enhanced chemical vapor deposition (PECVD) for passivation of surface and sidewalls and as an antireflection coating. A thin (~10 nm) Ti adhesion layer was evaporated. Finally, Al was thermally evaporated on Ti to become the 200 nm thick top and bottom electrodes. Figure 5(a) shows the scanning electron microscope (SEM) image of the completed devices.
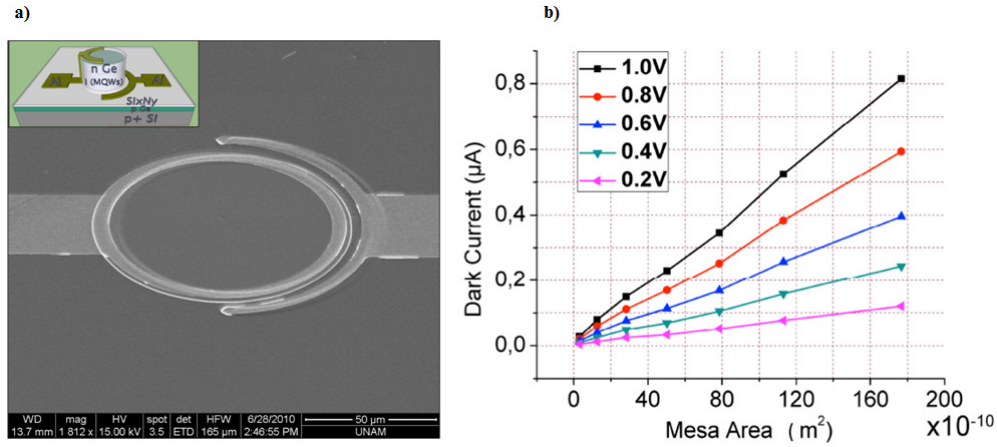
a)

b)

Fig. 5. (a) Scanning electron microscope (SEM) image of the completed *p-i-n* optical detector. The lower inset is an illustration of the device cross section, (b) Measured photodetector dark current as a function of mesa area at different bias voltages.

3. Optoelectronic characterization

Current output (I-V) and responsivity of these photodetectors as a function of voltage bias were measured to test the performance of the low temperature grown mesa shaped MQW photodetectors. Figure 5(b) shows the measured reverse leakage current with respect to mesa area. Linear relation between leakage current and mesa area indicates that the bulk leakage dominates surface leakage and the bulk component essentially determines total leakage. Responsivity of 0.1 A/W was measured at 1310 nm and 0V bias for the device with 120 µm mesa diameter. Table 2 shows the best-reported Si-Ge based *p-i-n* and an extremely efficient MSM photodetector responsivity performances and corresponding parameters.

Table 2. Reported Dark Current Density and Responsivity Values from Literature

Structure	Ge Thickness (µm)	Dark Current (mA/cm^2)	Responsivity (A/W)		Wave guide	Growth Technique	Tun able	Year Ref.
			1300 nm	1550 nm				
n-i Ge/p Si	4	15	0.89	0.75	No	UHVCVD + annealing	-	2002 [11]
n-i Ge/p Si	1	1000	-	1.08	Yes	UHVCVD + annealing	-	2007 [12]
i Ge/Si (MSM)	4.5	100	-	0.85	No	RPCVD + annealing	-	2006 [3]
Ge on n-Si	1	1				UHVCVD + annealing	-	2001 [20]
p-Ge/n-Si	0.2	0.3				MBE	-	2004 [21]
Ge on-Si	1.4	1.7				RPCVD	-	2007 [22]
MQW SiGe	0.3	10	0.12	0.01	No	RPCVD + annealing	Yes	This work

For the devices with 20 µm and 120 µm mesa diameters, reverse leakage current of 32 nA and 1.27 µA at −1V bias was measured, respectively, which correspond to ~10 mA/cm^2 leakage current density. This value is comparable with reported values for *p-i-n* photodetectors in the literature, listed in Table 2. The bulk current dominates the total dark current verified by the linear relation between the dark current density obtained from different mesa area devices, which is attributed to low surface leakage. Photocurrent data was acquired with chopped xenon light bulb source with a 12.5 cm monochromator with a 600 lines mm^{-1} grating, and a lock-in amplifier. Figure 6 plots the acquired spectral response of a 80-µm-diameter device for different applied reverse bias voltages. Measured responsivity values in excess of 100 mA/W are obtained in the 1300-1600 nm spectral range. The responsivity could be further increased by MQW layer thickness, which may limit device speed. Assuming a fully depleted intrinsic layer (300 nm), carrier transit time would be in the order of a few picoseconds. For devices with areas less than 100 square microns, the *RC* time constant is estimated to be less than a picosecond (50 Ω resistance and 0.35 fF/cm^2 detector capacitance per unit area), suggesting that device speed is limited by carrier transit time, though no measurements were performed to verify this claim. The spectral responsivity of the fabricated optical devices can be tuned by the applied reverse bias as shown for reverse bias voltages in Fig. 6. The absorption edge of the devices can be shifted by several tens of nanometers by applying few volts (<3 V) which is promising for low cost integration. It may be possible to use cavity or plasmonic resonance to increase the field intensity in the absorbing layer, to further improve device responsivity without limiting the carrier transit time.
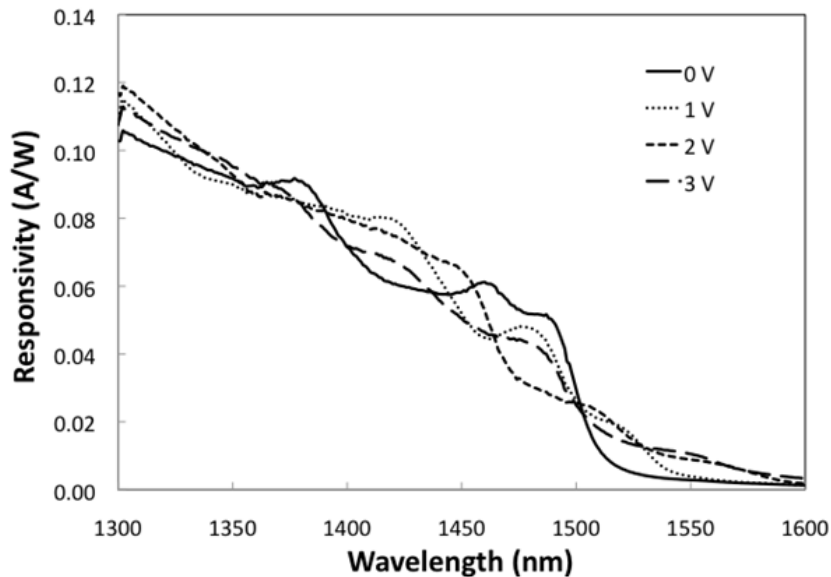

Fig. 6. Measured spectral responsivity of fabricated devices with a mesa diameter of 80 µm.

In conclusion, mesa structured *p-i-n* photodetectors based on SiGe multi quantum well absorbing layers with voltage-tunable spectral response are experimentally demonstrated. Single crystal SiGe multi quantum well layers with low dislocation-density are grown on Silicon substrates by MHAH technique, enabling compatibility with III-V optoelectronics and Silicon VLSI technology. Nanostructural characterization indicates that high quality quantum well layers are formed. Experimental results from fabricated photodetector devices show moderate responsivity values of about 0.1 A/W and low dark current density of approximately 10 mA/cm^2. In addition, voltage-tunable spectral response is also

demonstrated. Integration of such voltage-tunable photodetectors with low cost Si technology is promising for added optical functionality for VLSI devices.

Acknowledgments